Histol Histopathol (2025) 40: 1051-1060

Histology and Histopathology
From Cell Biology to Tissue Engineering

ORIGINAL ARTICLE Open Access

Gradual expression of MMP9 and MT1-MMP at the tumor-stroma interface in head and neck squamous cell carcinoma

Stefan Rusu[1,2*], Vincent Nuyens[3*], Alexandre Rousseau[3], Philippe Lothaire[4], Nathalie Nagy[5], Karim Zouaoui Boudjeltia[3] and Pierrick Uzureau[3]

[1]Department of Pathology, Hôpital Universitaire de Bruxelles, CUB Hôpital Erasme, Université Libre de Bruxelles, Brussels, [2]Centre Universitaire Inter Régional d'Expertise en Anatomie Pathologique Hospitalière, Charleroi, [3]Laboratory of Experimental Medicine, [4]Department of Surgery and [5]Department of Pathology, Centre Hospitalier Universitaire de Charleroi-Chimay, Université Libre de Bruxelles, Montigny-le-Tilleul, Belgium

*These authors contributed equally to this work

Summary. Due to the late-stage diagnosis of head and neck squamous cell carcinoma (HNSCC), treatment remains a significant clinical challenge. The metalloproteinases MMP-9 and MT1-MMP play a pivotal role in extracellular matrix remodeling, thereby facilitating tumor growth and metastasis. Tumor progression requires the degradation of the basement membrane. The principal components of this structure, namely collagen IV and laminin, are the main targets of both MMP-9 and MT1-MMP. However, they can also exert influence over the expression of these enzymes. Oxidative stress plays an instrumental role in tumor development, functioning as a key inducer of metalloproteinase expression. The present study investigates the distribution of MMP-9 and MT1-MMP within tumor nests and along the basement membrane, comparing these with the distributions of collagen IV, laminin-332, and the antioxidant MnSOD. Biopsies from 12 patients with HNSCC and poor prognostic factors were subjected to immunofluorescence analysis. MMP-9 and MT1-MMP were found to be predominantly present in tumor cells, with a significant decrease in expression from the periphery to the center of tumor nests. Co-localization studies with laminin-332 and collagen IV, revealed substantial overlap, in accordance with the role of MMPs in basal membrane degradation. The cellular expression of laminin-332 associated with MMP-9 expression suggests an intricate relationship between metalloproteinases and their targets. While the previously observed pattern of glutathione-producing enzyme was similar to the metalloproteinases pattern, MnSOD expression was homogeneously distributed within tumor nests. Our findings reveal various distribution patterns of oxidative stress regulators, suggesting a complicated interplay in the development of HNSCC.

Key words: Matrix metalloproteinase, Basement membrane, Oxidative stress, Superoxide dismutase

Corresponding Author: Pierrick Uzureau, Laboratoire de Médecine Expérimentale, Hôpital André Vésale, Rue de Gozée 706, 6110 Montigny le Tilleul, Belgium. e-mail: pierrick.uzureau@humani.be
www.hh.um.es. DOI: 10.14670/HH-18-858

Introduction

Head and neck squamous cell carcinomas (HNSCCs) are the most prevalent malignant tumors of the head and neck (Sung et al., 2021). Progression to advanced stages is characterized by invasion of the surrounding tissues and ultimately, metastatic spread (Chow, 2020). To access the surrounding stroma, the tumor must first cross the basement membrane (BM). The primary components of this physical barrier are collagen IV and laminins. Collagen serves as the backbone, while laminins facilitate the connection between collagen and neighboring cells (Chang and Chaudhuri, 2019). In HNSCC, Laminin-111 and laminin-332 (Ln332) are the main isoforms associated with the aggressiveness of the tumor (Meireles Da Costa et al., 2021). Ln332 is specific to the epithelial BM, serving to bridge this structure to epithelial cells through its interaction with integrin α6β4 (Berndt et al., 2022). This isoform is secreted by tumor cells and has been linked to the malignant transformation of squamous tumors. Ln332 deposition in the extracellular matrix (ECM) is also associated with a poor prognosis and

treatment resistance (Meireles Da Costa et al., 2021). The degradation of collagen IV is associated with higher grades of oral squamous carcinoma (Agarwal and Ballabh, 2013). While collagen's triple-helical structure is typically resistant to proteases, *in vivo* collagen degradation is performed by members of the metalloproteinase (MMP) family (Chang and Chaudhuri, 2019).

The main function of MMPs is to dynamically remodel the ECM during development and wound healing in healthy organs (Cui et al., 2017). In cancer, the interaction between ECM and tumor cells is responsible for cell transformation and tumor growth (Koontongkaew, 2013; Henke et al., 2019). MMPs are highly expressed at every stage of cancer development (Wieczorek et al., 2015; Gobin et al., 2019). MMP-2, MMP-9, and MT1-MMP stand out as major factors in tumor growth, being overexpressed in most cancers, including HNSCC (Rosenthal and Matrisian, 2006; Gobin et al., 2019). Both MMP2 and MMP-9 are soluble gelatinases that degrade collagen IV and laminins, and also contribute to the release and activation of TGFβ, thereby promoting tumor growth (Giannelli et al., 1997; Sternlicht and Werb, 2001; Gu et al., 2005). MT1-MMP is a membrane-bound protease that has been identified as the key activator of MMP-2 (Sato et al., 1994). This protease has been demonstrated to degrade Ln332, and its activation of MMP-2 is crucial for collagen IV remodeling (Ohuchi et al., 1997; Meireles Da Costa et al., 2021). MT1-MMP is located on invadopodia, which disrupts the ECM and assists tumor infiltration of surrounding tissues (Itoh, 2015; Chang and Chaudhuri, 2019). MMP-9 and MT1-MMP have been extensively studied in HNSCC due to their potential as biomarkers and therapeutic targets (Sternlicht and Werb, 2001; Rosenthal and Matrisian, 2006). Although MMPs are typically produced by stromal cells in cancers, increased expression of MMP-9 and MT1-MMP has been reported in HNSCC tumor cells (Charous et al., 1997; Gonzalez-Avila et al., 2020). The relationship between MMP and Ln332 may be more intricate than initially assumed. It has been previously demonstrated that Ln332 is capable of inducing MT1-MMP in thymocytes (Vivinus-Nebot et al., 2004). Recently, Ln332 fragments have been demonstrated to induce MMP9 expression in keratinocytes during the wound-healing process. Notably, the observed MMP-9 activity was shown to be dependent on MT1-MMP (Michopoulou et al., 2020). Further investigation is required to elucidate whether the spatial distribution of these BM proteins in tumors may be influenced by Ln332 production.

Another factor that impacts MMP levels in cancers is oxidative stress, which can act as a double-edged sword in the process of tumorigenesis (Reuter et al., 2010). The impact of oxidative stress on tumorigenesis is dependent on the level of stress, the targets affected, and the timing of the event in question (Chio and Tuveson, 2017). The primary effectors of oxidative stress are reactive oxygen species (ROS), which are generated by the mitochondrial respiratory chain (Huang and Pan, 2020). Within tumors, these highly reactive molecules alter the ECM structure, modulate inflammation, and directly impact cell proliferation and death (Reuter et al., 2010; Chio and Tuveson, 2017). Notably, ROS and nitric oxide can directly activate MMP-9 through the oxidation of cysteine residues, thereby establishing a direct correlation between oxidative stress levels and MMP-9 activity (Huang, 2018). The regulation of oxidative stress represents a crucial process for cells. The antioxidant system is dependent on the detoxification of ROS through superoxide dismutase (SOD) and glutathione (GSH) (Chio and Tuveson, 2017; Jena et al., 2023). Given its mitochondrial localization, MnSOD represents a crucial component of the antioxidant system. As MnSOD is overexpressed in HNSCC cells and is associated with increased tumor metastasis, it was postulated that these tumor cells may experience elevated levels of oxidation as a consequence of their high proliferative activity

Table 1. Clinicopathological data of included patients.

No.	Gender	Age	Localization	Histologic grade[a,b]	pTNM[a,c]	Tumor size (mm)[a]	Invasion depth (mm)[a]	LVI	PNI
1	M	73	Mobile tongue	I	T2N0	15	10	+	+
2	M	45	Palate	I	T3N3b	40	25	+	+
3	M	62	Mobile tongue	I	T3N1	25	12	+	-
4	M	57	Palate	I	T4aN0	25	12	-	+
5	H	61	Larynx	I	T4aN1	70	NS	+	+
6	M	59	Mobile tongue	I	T2N0	35	9	-	+
7	M	61	Palate	I	T2N0	45	4	-	+
8	F	73	Mobile tongue	II	T4aN2c	70	35	+	NS
9	F	70	Palate	II	T4aN3b	60	30	+	+
10	M	69	Larynx	II	T2N2b	30	ns	+	+
11	F	57	Oropharynx	III	T3N0	45	30	+	+
12	M	69	Palate	III	T4aN1	15	12	+	NS

[a]: Histological analyses were performed on surgical specimens acquired from the patients. [b]: Squamous cell carcinomas were graded histologically as follows: I- well differentiated, II- moderately differentiated, and III- poorly differentiated. [c]: Pathologic Classification followed the Union for International Cancer Control (UICC) TNM classification, 8th edition (2017). LVI, lymphovascular invasion. PNI, perineural invasion. M, male. F, female. +, present. -, absent. NS, not specified.

(Piyathilake et al., 2002; Hempel et al., 2011). The biosynthesis of glutathione (GSH) is a two-step process that is mediated by glutamate-cysteine ligase (GCL) and glutathione synthetase, where GCL is the rate-limiting enzyme of GSH biosynthesis (Jena et al., 2023). We previously reported that glutamate cysteine ligase (GCL) is overexpressed in regions of tumor nests where cells demonstrate proliferative activity (Dequanter et al., 2016). These regions are situated at the tumor nest periphery, adjacent to the BM, and are, therefore, anticipated to be primary contributors to MMP production.

In this study, we investigated the spatial correlation between MMP-9 and MT1-MMP, Ln332 and oxidative stress. To do so, we evaluated the distribution pattern of MMPs in tumor nests relative to the tumor-stroma interface and compared this pattern to that of Ln332, a BM marker, collagen IV, and MnSOD.

Materials and methods

Ethical statements

This study was approved by the Ethics Committee of the University Hospital Center of Charleroi, Intercommunale de Santé Publique du Pays de Charleroi (ISPPC) (registration number OM008), located in Montigny le Tilleul, Belgium. This approval corresponds to Compliance Certification Board Numbers B32520107991 and B325201111821.

Sample procurement

Fresh tumor tissue samples were obtained from 22 patients who underwent surgical resection for HNSCC at the University Hospital Center of Charleroi, Hôpital André Vésale, in Montigny-le-Tilleul, Belgium, from 2011 to 2018 (Table 1). Of the 22 patients initially enrolled in the study, one patient was excluded due to prior neoadjuvant therapy, and 9 were later excluded due to artifacts on the tissue slides related to fulguration, microtomy, staining, or mounting (Fig. 1). Twelve patients were included in the study, and five series of measurements were conducted based on single or double immunofluorescence (IF) staining.

Immunofluorescence staining

Fresh tissue samples from surgical resections were embedded in OCT (Sakura Fine Technical, Tokyo, Japan) using a tissue mold, and stored at -80°C with a Clini-Rapid Freezer machine (Bright Instrument Company Ltd., Huntingdon, UK). The tissue was sectioned into 7 µm-thick slices using a Leica CM1900 cryostat (Nussloch GmbH). Two single IF series and three double IF series were performed on the embedded tissue (Fig. 1). The analyzed markers included MMP9, MT1-MMP, collagen, laminin, and MnSOD. The antibodies used for IF staining are listed in Table 2.

The tissue slides were fixed with 2% para-formaldehyde for 2 minutes, followed by methanol at

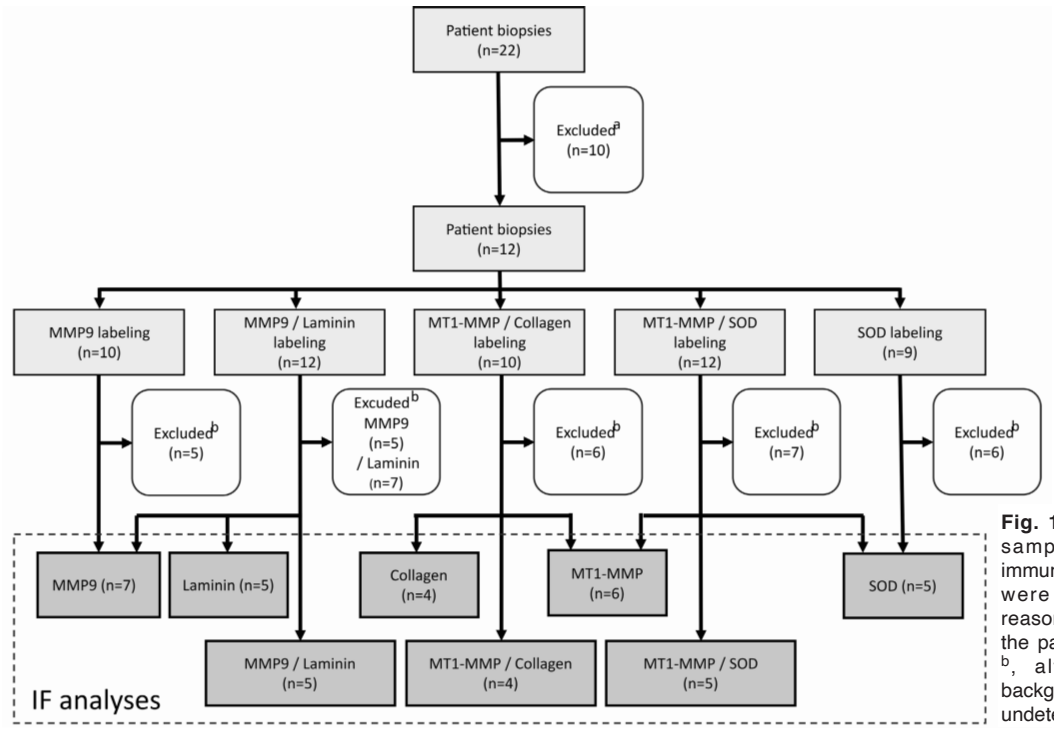

Fig. 1. Flow chart summarizing the sample collection process (IF, immunofluorescence). Patient biopsies were excluded for the following reasons: [a], neoadjuvant treatment of the patient, slide processing artifacts; [b], altered tissue section, high background fluorescence, and weak or undetectable signal.

-20°C for 10 minutes. After three washes with 1 mM Tris-buffered saline pH 8 (TBS), the tissues were permeabilized with 0.5% Triton X-100 for 10 minutes. After the slides were washed three times with TBS and blocked using 5% Bovine Serum Albumin (BSA) for 30 minutes at 37°C, they were incubated with the first primary antibody overnight at 4°C. Following three 5-minute washes with TBS, the tissue slides were incubated with the secondary antibody for 45 minutes at 37°C.

For double IF staining, TBS-washed slides were fixed in 2% paraformaldehyde for 10 minutes, washed again with TBS, and blocked with 5% BSA for 30 minutes at 37°C. The tissue slides were then incubated with the second primary antibody overnight at 4°C, followed by three more 5-minute washes with TBS. The slides were then incubated with the second secondary antibody for 45 minutes at 37°C. After four additional 5-minute washes, they were dehydrated in 70%, 85%, and then 96% isopropanol. The slides were air-dried and mounted using a solution containing 90% glycerol, 1% anti-fading agent, 8% TBS, and 1 µg/ml diamidino phenylindole (DAPI). Once images had been acquired, all slides were counterstained with hematoxylin and eosin (HE). Negative controls, in which one or both primary antibodies were absent, were conducted on serial sections to guarantee the specificity of labeling.

Image acquisition, processing, and measurements

The slides were scanned with a Nikon Eclipse Ti Fluorescence Microscope equipped with a Nikon CFI Plan Fluor 10x objective (Nikon Instruments Inc, NY, USA). The HE and IF images were aligned using the Data Science for Health Image Alignment plugin in ImageJ software (National Institute of Health, Bethesda, MD, USA). A trained pathologist used HE images to delineate tumor nests. Exclusion criteria included tumor nests located at the border of the tissue sample and tumor nests with artifacts from tissue sectioning, embedding, or staining. The subtraction method was employed to minimize background fluorescence to zero, and noise reduction was achieved through median filtering. Maximum pixel intensity was standardized across all images using the multiplication method. The mean fluorescence signal intensity was calculated in regions of interest (ROIs) on an 8-bit scale. ROIs consisted of concentric areas with a width of 10 µm, ranging from the edge to the center of each tumor nest as well as from the periphery of the nest towards the ECM (Fig. 2).

Statistical analysis

Statistical analyses were performed using Prism software (GraphPad Software, San Diego, CA, USA, www.graphpad.com). The distribution of IF labeling at the tumor-stroma interface was evaluated using the Wilcoxon test. The IF labeling of tumor nests was assessed via Friedman analysis of variance by ranks and the Nemenyi test was used for pairwise comparisons. *p*-values were adjusted for multiple analyses. The colocalizations were evaluated using Pearson's coefficient and Mander's overlap coefficient in ImageJ.

Data availability

The datasets analyzed in the present study are available upon reasonable request from the corresponding author.

Results

Clinicopathological data

Twelve patients were enrolled in the study, consisting of nine males and three females. Their clinicopathological data are summarized in Table 1. The median age at surgery was 62 years, with a range of 45 to 73 years. The majority of tumors, five cases, were located in the palate, while four were found in the mobile tongue, two in the larynx, and one in the oropharynx. Pathological evaluation indicated seven well-differentiated, three moderately differentiated, and two poorly differentiated cases of squamous cell carcinoma. The median tumor size was 38 mm, with a range of 15-70 mm. Notably, poor histological prognostic factors were often present, such as lymphovascular invasion in 9 out of 12 cases, perineural invasion in 9 out of 10 cases, and lymph node

Table 2. Antibodies used for immunofluorescence staining.

Antibody	Primary/ Secondary	Dilution	Provider	Reference
Recombinant Rabbit monoclonal Anti-MMP-9 antibody [EP 1255y]	Primary	1/500	Abcam (Cambridge, UK)	ab 137867
Recombinant Rabbit monoclonal Anti-MMP-14 antibody [EP 1264y]	Primary	1/500	Abcam (Cambridge, UK)	ab 51074
Mouse monoclonal anti-Collagen-IV Antibody (1042)	Primary	1/1000	Thermo Fisher Scientific (Waltham, Ma, USA)	14-9871-37
Mouse monoclonal Anti-Laminin-5 antibody [P3H9-2]	Primary	1/500	Abcam (Cambridge, UK)	ab78286
Mouse monoclonal Anti-MnSOD (MnS-1)	Primary	1/200	Thermo Fisher Scientific (Waltham, Ma, USA)	BMS 122
Alexa Fluor ® 488 goat Anti-Rabbit IgG	Secondary	1/2500	Thermo Fisher Scientific (Waltham, Ma, USA)	A11034
Alexa Fluor ® 488 goat Anti-Mouse IgG	Secondary	1/2500	Thermo Fisher Scientific (Waltham, Ma, USA)	A11029
Alexa Fluor ® 594 donkey Anti-Rabbit IgG	Secondary	1/2500	Thermo Fisher Scientific (Waltham, Ma, USA)	A21207
Alexa Fluor ® 594 goat Anti-Mouse IgG	Secondary	1/2500	Thermo Fisher Scientific (Waltham, Ma, USA)	A11032

involvement in 7 out of 12 cases.

MMP9 and MT1-MMP expression increased at the periphery of tumor nests

In this study, we investigated the distribution of MMP9 and MT1-MMP within the immediate tumor nest surroundings. HE staining was used to outline the tumor nests (Fig. 2). IF was performed to analyze MMP9 and MT1-MMP expression on a total of 88 and 62 tumor nests, respectively. MMP labeling was mostly located within tumor cells, where MMP9 was detected in the cytoplasm and MT1-MMP at the plasma membrane (Fig. 3, second column of panels). Lower expression of MMPs was observed in the stroma, specifically in fibroblasts, endothelial cells, macrophages, and inflammatory cells. MMP9 and MT1-MMP both demonstrated a decreasing pattern across 10-µm intervals extending from the edge of the tumor nest lined by the BM, towards the central area ($p<0.0001$, see Fig. 3A, second panel and 4A for MMP9 and Fig. 3B,C, second panels and 4C for MT1-MMP). Observation of the 10-µm inner and 10-µm outer areas of the tumor nest boundary revealed that MMP9 expression was significantly higher at the inner periphery of the tumor nest when compared with the adjacent stroma (Fig. 3A, second panel; Fig. 4A). Although statistically significant, the measured expression of MT1-MMP in these regions only demonstrated a 5% difference between the 0-10 µm Tumor and 0-10 µm Stroma range (Fig. 4C). Additionally, the signal in the latter region was significantly higher than in the 20-µm distant areas of the ECM. In both cases, the highest level of expression was observed within a 10-µm ring located in the outermost region of the tumor nest. Within this cell layer, elevated expression of both MMPs was observed at the cell surface lining the BM (Fig. 3, arrows).

MMP9 and MT1-MMP overlapped with the basement membrane

Within the BM of epithelial cells, Ln332, which can be produced by tumor cells, was shown to induce the expression of MMP9 during wound healing. To evaluate this pathway in tumor cells, the spatial correlation between MMP9, MT1-MMP, Ln332, and the BM marker, collagen IV, was investigated. The expression of the two BM proteins was analyzed in 46 tumor nests for the MMP9-laminin IF series and 32 tumor nests for the MT1-MMP-collagen IF series. Ln332 labeling revealed a continuous but variable thickness pattern, while collagen IV exhibited a sporadic expression pattern with varying intensities (Fig. 3A,B, third panels). Both markers delineated the boundaries of the tumor nest, indicating that they constituted part of the BM surrounding the nest. The highest levels of expression were observed in the 0-10-µm range in the stroma (Fig. 4B,D). Compared with the surrounding region, the signal intensity for Ln332 and collagen IV in the tumor nest was observed to be 2.5-fold and 4-fold lower, respectively (Fig. 4B,D). A faint but distinct signal was observed for Ln332 within the first cell layers of the tumor nest lining the BM. Conversely, no such signal could be observed for collagen IV (Fig. 3B, third panel), demonstrating the specificity of this cellular expression of Ln332. Furthermore, these regions were found to correspond with areas exhibiting increased MMP9 expression (Fig. 3A, third panel).

To assess the colocalization of BM components and MMPs, both Pearson's coefficient and Manders' overlapping coefficient were employed. The results indicate that MMP9 with Ln332 and MT1-MMP with collagen IV had notable colocalization with Pearson coefficient values of 0.48±0.11 and 0.43±0.08, respectively. While Ln332 and collagen IV were

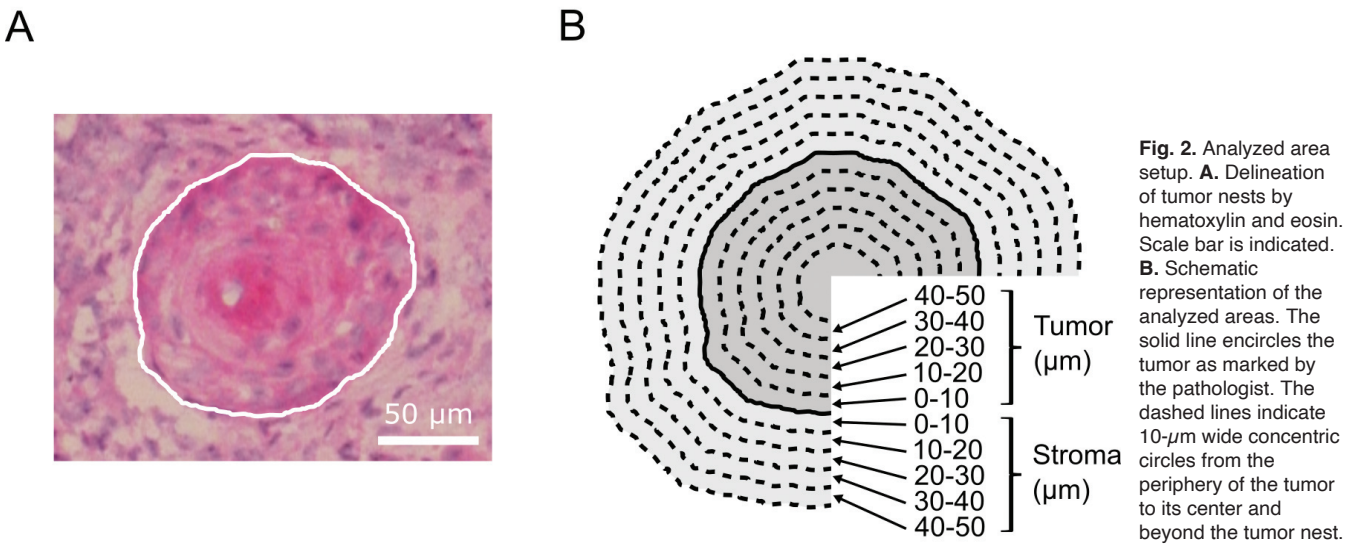

Fig. 2. Analyzed area setup. **A.** Delineation of tumor nests by hematoxylin and eosin. Scale bar is indicated. **B.** Schematic representation of the analyzed areas. The solid line encircles the tumor as marked by the pathologist. The dashed lines indicate 10-μm wide concentric circles from the periphery of the tumor to its center and beyond the tumor nest.

restricted to a small area around the tumor nest, MMP9 and MT1-MMP labeling extended to a large part of the tumor nest (Fig. 3). Thus, the average Manders' coefficients for laminin and collagen in relation to MMPs were 44% and 60%, respectively (Fig. 5A,B). Conversely, the mean Manders' coefficients of MMP9 and MT1-MMP concerning the BM components were 27% and 21%, respectively. These findings indicate that while MMPs did overlap with Ln332 and collagen IV, they were not confined to that region.

MnSOD pattern differed from the MMP distribution

In previous research, we investigated the distribution of a Glutamate-Cysteine Ligase (GCL) subunit in tumors of the head and neck (Dequanter et al., 2016). GCL plays a crucial role in glutathione synthesis and thus indicates the anti-oxidant activity of cells (Gorrini et al., 2013). GCL expression was increased in the tumor nest periphery when compared with the central area and adjacent stroma. The distribution of GCL was analogous to that of MMP9 and MT1-MMP observed in the present study (Dequanter et al., 2016). We examined the correlation between the MMPs and oxidative stress markers using MnSOD. Unlike GCL, which is a component of glutathione's biosynthesis chain, MnSOD directly contributes to free radical detoxification (Miao and St. Clair, 2009). The expression of MnSOD was analyzed in 40 tumor nests, finding that it was primarily present in the cytoplasm and was significantly more abundant in tumor nests compared with adjacent stroma (Fig. 3C). Contrary to MMPs and GCL, MnSOD exhibited a predominantly uniform distribution within tumor nests (Fig. 4E). Despite this divergent pattern, MnSOD and MMPs showed extensive colocalization in the 34 tumor nests analyzed. Indeed, the Pearson

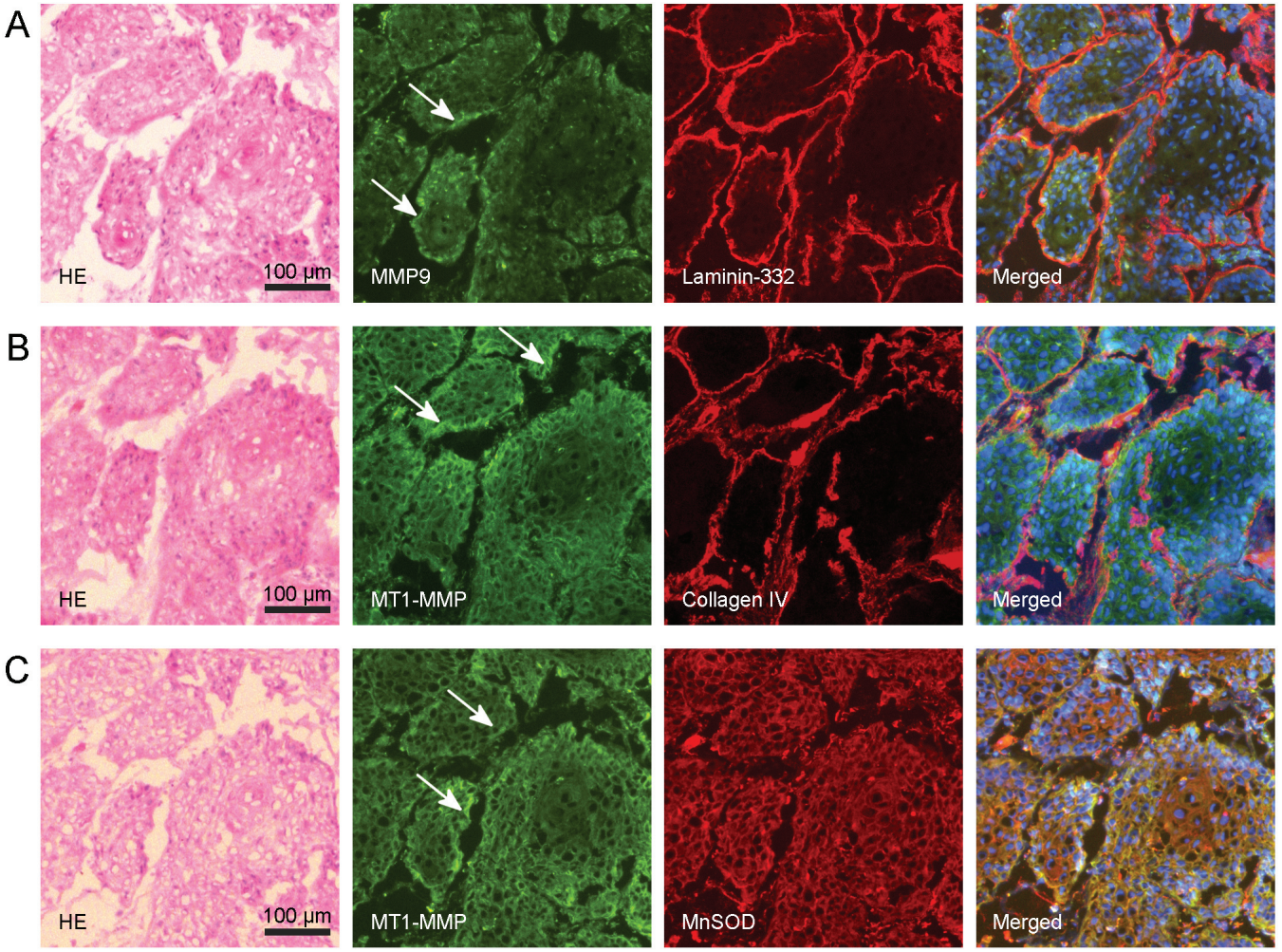

Fig. 3. MMP9, MT1-MMP, laminin-332, collagen IV, and SOD labeling. Rows A, B, and C show three serial sections of the biopsy from patient 6. Hematoxylin and eosin staining is shown in column 1. MMP9, MT1-MMP, laminin-332, collagen IV, and SOD staining are shown in columns 2 and 3. Merged labeling of DAPI staining with MMP9 and laminin-332 **(A)**, MT1-MMP and collagen IV **(B)**, and MT1-MMP and SOD **(C)** is shown in the last column. The 50-*µ*m scale bar is indicated in the hematoxylin and eosin staining panel. Panels in each row are shown at the same scale.

coefficient was 0.70+/-0.12, and the Manders coefficient revealed that 70% of MT1-MMP colocalized with MnSOD, while over 50% of MnSOD overlapped with MT1-MMP (Fig. 5C).

Discussion

Matrix metalloproteinases play a critical role in tumorigenesis and metastasis. Although they are

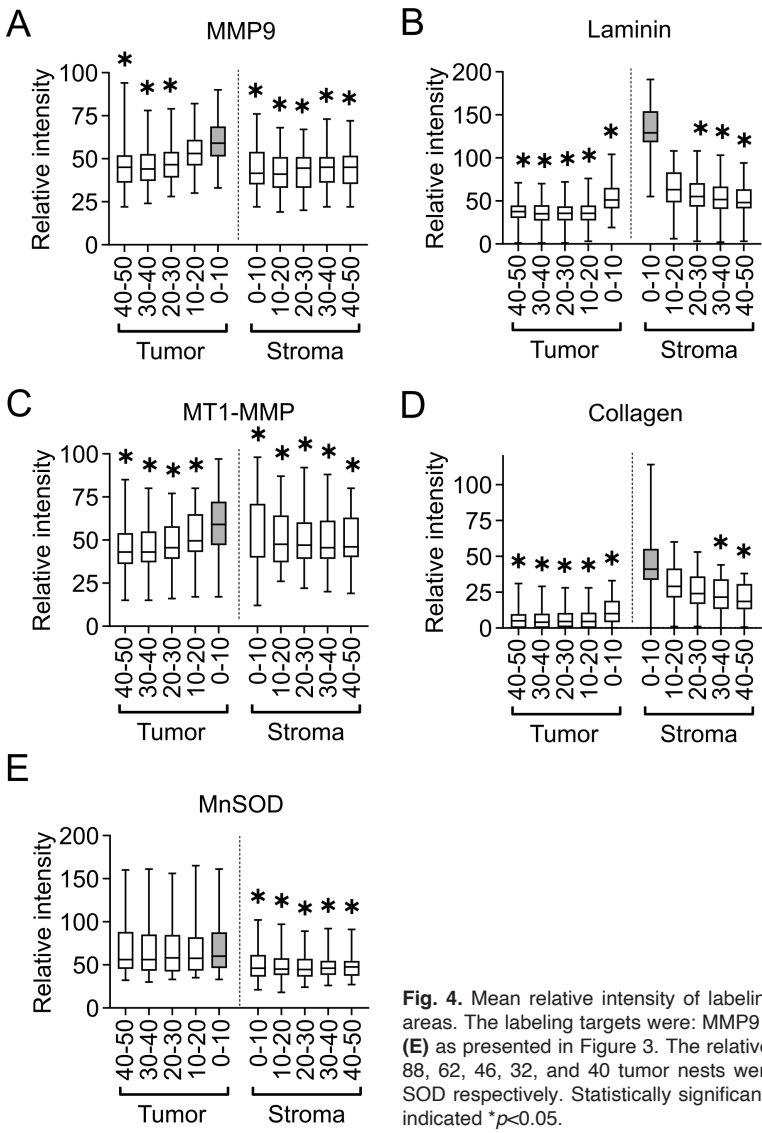

Fig. 4. Mean relative intensity of labeling in 10-μm wide concentric circles within the tumor and stromal areas. The labeling targets were: MMP9 **(A)**, MT1-MMP **(B)**, laminin-332 **(C)**, collagen IV **(D)**, and MnSOD **(E)** as presented in Figure 3. The relative distance to the delineated nest is shown on the x-axis. A total of 88, 62, 46, 32, and 40 tumor nests were analyzed for MMP9, MT1-MMP, laminin-332, collagen IV, and SOD respectively. Statistically significant differences with the highest median intensity (grey box plot) are indicated *p<0.05.

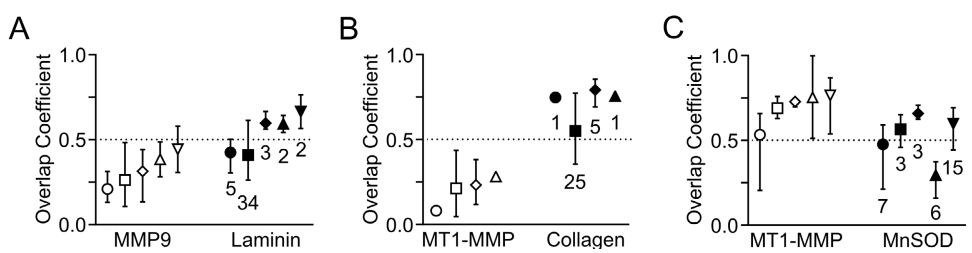

Fig. 5. Colocalization of double immunofluorescence labeling of MMP9 with laminin-332 **(A)**, MT1-MMP with Collagen IV **(B)**, and MT1-MMP with MnSOD **(C)**. Each symbol in the graph represents a patient biopsy. The medians of the Manders' overlap coefficient of the green and red labeling are displayed as open and closed symbols, respectively. The range from the minimum to maximum values is also shown. The number of tumor nests analyzed for each patient is presented underneath each symbol.

involved in BM degradation, which enables tissue invasion and metastasis, MMPs are active at various stages of tumor progression. MMP-9 and MT1-MMP are involved in BM degradation via direct action or MMP-2 activation (Kessenbrock et al., 2010). Recent reports indicate that Ln332, a laminin specific to the epithelial BM, exerts an effect on the expression of these enzymes (Vivinus-Nebot et al., 2004; Michopoulou et al., 2020). This study aimed to compare the distribution of Ln332 and MMP-9 and MT1-MMP in HNSCC. Our findings indicate that tumor cells predominantly express these proteases, although stromal cells also contribute to the expression. The observed increase in expression is consistent with previous reports in HNSCC, although stromal cells are typically the primary producers in other cancers (Rosenthal and Matrisian, 2006; Kessenbrock et al., 2010). However, in contrast with previous reports, our findings revealed a non-homogeneous distribution of these proteases within the tumor nests (Kurahara et al., 1999). Both MMP-9 and MT1-MMP were predominantly located at the inner periphery of the nests, lining the BM boundary. In the stroma, their pattern was restricted to some stromal cells but homogeneously spread. The subcellular localization of MMP-9 and MT1-MMP, respectively, in the whole cell and at the cell periphery, was consistent with their expected roles, as MMP-9 is a soluble protease and MT1-MMP is membrane-bound. To the best of our knowledge, no evaluation of the MMP distribution within tumor nests has been conducted thus far. This represents the first report of an MMP gradient towards the interface between the tumor and stroma. Previous studies have established that no difference in the expression of MMPs could be observed between the center and margin of the tumor (Charous et al., 1997). However, this study analyzed MMP expression in the resection margin compared with the core of the tumor, while current research focused on the cellular interface between the tumor and stroma.

Our findings indicated that tumor cells within HNSCC produce the BM components collagen IV and laminin-332, as evidenced by the observed distribution around most nests and the relative thickness of both labelings. An increase in the expression of collagen and laminin has been documented in certain tumors, where these proteins are known to play a critical role in tumor transformation (Henke et al., 2019; Meireles Da Costa et al., 2021). The discontinuity of the BM pattern observed in the present study is in accordance with previous studies, demonstrating discontinuity of laminin and collagen in high-grade tumors (Kannan et al., 1994; Santos-García et al., 2006). Although disruption of the BM has been associated with poorer prognoses, not all aggressive cases exhibited discontinuity of the BM around tumor nests (Santos-García et al., 2006; Chang and Chaudhuri, 2019). At the whole tumor level, degradation of the ECM has been associated with increased expression of MMPs (Kurahara et al., 1999). In the present study, MMP-9 was observed to overlap half of the laminin surface, while MT1-MMP demonstrated a strong superimposition on collagen. The alignment of MMPs and BM is consistent with the protease's crucial role in ECM remodeling (Kessenbrock et al., 2010; Koontongkaew, 2013). MMP-9 was not detected within the stroma, including BM. Conversely, MT1-MMP demonstrated significant expression on the outer side of the nest. The possibility of delineation errors associated with the BM was excluded, as laminin and collagen were positioned within the first outer ring. However, this discrepancy may be attributed to challenges in accurately defining the nests, particularly in light of the resolution of the analyzed concentric ring and the indistinct tumor outlines in certain biopsies. It is noteworthy that Ln332 was detected at the membrane of tumor cells, whereas collagen IV was not. Ln332 was detected in cells displaying the highest levels of MMP9 expression. As Ln332 can be produced by tumor cells, a hypothesis could be formed that Ln332 produced by the tumor nest periphery induces MMP9 expression, contributing to the degradation of the BM around the nest (Michopoulou et al., 2020; Berndt et al., 2022).

In addition, the uneven distribution of MMP within the tumor should be considered in the context of the oxidative stress pattern. Previously, we reported a corresponding trend for GCL, the crucial enzyme for GSH synthesis, indicating a gradient of oxidative stress from the tumor center to the tumor-stroma interface (Dequanter et al., 2016). It is postulated that the invasion of surrounding tissues with concomitant increased ECM degradation is a primary factor contributing to increased oxidative stress. Of note, both MMP-9 and MT1-MMP expression have been demonstrated to undergo induction by oxidative stress *in vitro* (Galli et al., 2005; Yu et al., 2008). This suggests that the observed MMP pattern may result from increased oxidative stress at the tumor-stroma interface. Although MMP activity was not monitored in this study, it is notable that MMP-9 can be chemically activated through GSH levels (Okamoto et al., 2001). Furthermore, the outer regions of tumor nests display elevated rates of cell proliferation, which may also contribute to the overexpression of MMPs (Dequanter et al., 2016). Thus, the ECM applies a physical constraint on the expanding tumor, which the invadopodia developed by the tumor cells can alleviate by releasing MMP-9 and presenting MT1-MMP on their surface (Chang and Chaudhuri, 2019). These MMPs have been demonstrated to modulate tumor growth in mouse models by acting on growth factor levels and angiogenesis (Wieczorek et al., 2015). Both MMP-9 and MT1-MMP activate TGFβ, and MMP-9 cleaves growth factor-binding proteins that regulate the bioavailability of TGFβ and insulin-like growth factor (Kessenbrock et al., 2010; Gialeli et al., 2011). This observation may account for the widespread expression of MMP-9 and MT1-MMP in the proliferative regions of tumor nests.

In agreement with previous studies, an increase in the expression of MnSOD, which acts as the primary ROS scavenger, was observed in the biopsies (Piyathilake et al., 2002; Hempel et al., 2011). However,

the distribution of MnSOD did not correspond with that of GCL observed in our earlier research, nor did it align with that of MMPs (Dequanter et al., 2016). While the two signals coincided, their pattern differed with MnSOD exhibiting constant expression up to 50 µm away from the edge of the nest. Given that mitochondria are the primary source of ROS, the increased proliferative activity would lead to increased ROS production, which would in turn result in elevated MnSOD levels (Chio and Tuveson, 2017). These conclusions are in line with the results presented in the current study. Global oxidative stress results from a balance between ROS generators and the main antioxidant systems, SOD and GSH (Lv et al., 2019; Huang and Pan, 2020). It is likely that while mitochondrial activity is elevated in the peripheral areas of the nest, ROS are generated throughout the nest, accounting for the variance between GCL and MnSOD profiles. This observation implies that tumor cells exhibit varying phenotypes within nests. While all cells can confront ROS production and regulate oxidative stress, peripheral cells engaged in proliferation demonstrate the associated induction of MMPs and GSH to combat the oxidative stress caused by the tumor-stroma interaction.

In conclusion, our results demonstrated that the distribution of MMP-9 and MT1-MMP in tumor nests was not homogeneous, with increased expression observed at the tumor-stroma interface. This pattern coincided with the production of the major oxidative stress regulator but may also be a consequence of the intricate relationship between MMP and BM components. The discrepancies observed in cellular phenotypes concerning MMP production, oxidative stress response, and cell proliferation within a tumor nest provide novel insights into the pathogenesis of head and neck squamous cell carcinoma.

Acknowledgements. This research was supported by grants from the CHU Charleroi and the Fonds pour la Recherche Médicale en Hainaut (FRMH).

Conflict of interest statement. The authors declare no competing interests.

References

Agarwal P. and Ballabh R. (2013). Expression of type IV collagen in different histological grades of oral squamous cell carcinoma: An immunohistochemical study. J. Can. Res. Ther. 9, 272-275.

Berndt A., Gaßler N. and Franz M. (2022). Invasion-Associated reorganization of laminin 332 in oral squamous cell carcinomas: The role of the laminin γ2 chain in tumor biology, diagnosis, and therapy. Cancers 14, 4903.

Chang J. and Chaudhuri O. (2019). Beyond proteases: Basement membrane mechanics and cancer invasion. J Cell Biol. 218, 2456-2469.

Charous S.J., Stricklin G.P., Nanney L.B., Netterville J.L. and Burkey B.B. (1997). Expression of matrix metalloproteinases and tissue inhibitor of metalloproteinases in head and neck squamous cell carcinoma. Ann. Otol. Rhinol. Laryngol. 106, 271-278.

Chio I.I.C. and Tuveson D.A. (2017). ROS in cancer: The burning question. Trends Mol. Med. 23, 411-429.

Chow L.Q.M. (2020). Head and Neck Cancer. N. Engl. J. Med. 382, 60-72.

Cui N., Hu M. and Khalil R.A. (2017). Biochemical and biological attributes of matrix metalloproteinases. Prog. Mol. Biol. Transl Sci. 147, 1-73.

Dequanter D., Van de Velde M., Bar I., Nuyens V., Rousseau A., Nagy N., Vanhamm L., Vanhaeverbeek M., Brohee D., Delree P., Zouaoui Boudjeltia K., Lothaire P. and Uzureau P. (2016). Nuclear localization of glutamate-cysteine ligase is associated with proliferation in head and neck squamous cell carcinoma. Oncol. Lett. 11, 3660-3668.

Galli A., Svegliati-Baroni G., Ceni E., Milani S., Ridolfi F., Salzano R., Tarocchi M., Grappone C., Pellegrini G., Benedetti A., Surrenti C. and Casini A. (2005). Oxidative stress stimulates proliferation and invasiveness of hepatic stellate cells via a MMP2-mediated mechanism. Hepatology 41, 1074-1084.

Gialeli C., Theocharis A.D. and Karamanos N.K. (2011). Roles of matrix metalloproteinases in cancer progression and their pharmacological targeting. FEBS J. 278, 16-27.

Giannelli G., Falk-Marzillier J., Schiraldi O., Stetler-Stevenson W.G. and Quaranta V. (1997). Induction of cell migration by matrix metalloprotease-2 cleavage of laminin-5. Science 277, 225-228.

Gobin E., Bagwell K., Wagner J., Mysona D., Sandirasegarane S., Smith N., Bai S., Sharma A., Schleifer R. and She J.-X. (2019). A pan-cancer perspective of matrix metalloproteases (MMP) gene expression profile and their diagnostic/prognostic potential. BMC Cancer 19, 581.

Gonzalez-Avila G., Sommer B., García-Hernández A.A. and Ramos C. (2020). Matrix metalloproteinases' role in tumor microenvironment. Adv. Exp. Med. Biol. 1245, 97-131.

Gorrini C., Harris I.S. and Mak T.W. (2013). Modulation of oxidative stress as an anticancer strategy. Nat. Rev. Drug Discov. 12, 931-947.

Gu Z., Cui J., Brown S., Fridman R., Mobashery S., Strongin A.Y. and Lipton S.A. (2005). A highly specific inhibitor of matrix metalloproteinase-9 rescues laminin from proteolysis and neurons from apoptosis in transient focal cerebral ischemia. J Neurosci. 25, 6401-6408.

Hempel N., M. Carrico P. and Melendez J.A. (2011). Manganese superoxide dismutase (Sod2) and redox-control of signaling events that drive metastasis. Anticancer Agents Med. Chem. 11, 191-201.

Henke E., Nandigama R. and Ergün S. (2019). Extracellular matrix in the tumor microenvironment and its impact on cancer therapy. Front. Mol. Biosci. 6, 160.

Huang H. (2018). Matrix metalloproteinase-9 (MMP-9) as a cancer biomarker and MMP-9 biosensors: Recent advances. Sensors 18, 3249.

Huang G. and Pan S.-T. (2020). ROS-Mediated therapeutic strategy in chemo-/radiotherapy of head and neck cancer. Oxid. Med. Cell. Longev. 2020, 5047987.

Itoh Y. (2015). Membrane-type matrix metalloproteinases: Their functions and regulations. Matrix Biol. 44-46, 207-223.

Jena A.B., Samal R.R., Bhol N.K. and Duttaroy A.K. (2023). Cellular Red-Ox system in health and disease: The latest update. Biomed. Pharmacother. 162, 114606.

Kannan S., Balaram P., Chandran G.J., Pillai M.R., Mathew B., Nalinakumari K.R. and Nair M.K. (1994). Alterations in expression of basement membrane proteins during tumour progression in oral mucosa. Histopathology 24, 531-537.

Kessenbrock K., Plaks V. and Werb Z. (2010). Matrix metalloproteinases: Regulators of the tumor microenvironment. Cell 141, 52-67.

Koontongkaew S. (2013). The tumor microenvironment contribution to development, growth, invasion and metastasis of head and neck squamous cell carcinomas. J. Cancer 4, 66-83.

Kurahara S., Shinohara M., Ikebe T., Nakamura S., Beppu M., Hiraki A., Takeuchi H. and Shirasuna K. (1999). Expression of MMPS, MT-MMP, and TIMPs in squamous cell carcinoma of the oral cavity: Correlations with tumor invasion and metastasis. Head Neck 21, 627-638.

Lv H., Zhen C., Liu J., Yang P., Hu L. and Shang P. (2019). Unraveling the potential role of glutathione in multiple forms of cell death in cancer therapy. Oxid. Med. Cell. Longev. 2019, 1-16.

Meireles Da Costa N., Mendes F.A., Pontes B., Nasciutti L.E., Ribeiro Pinto L.F. and Palumbo Júnior A. (2021). Potential therapeutic significance of laminin in head and neck squamous carcinomas. Cancers 13, 1890.

Miao L. and St. Clair D.K. (2009). Regulation of superoxide dismutase genes: Implications in disease. Free Radic. Bio. Med. 47, 344-356.

Michopoulou A., Montmasson M., Garnier C., Lambert E., Dayan G. and Rousselle P. (2020). A novel mechanism in wound healing: Laminin 332 drives MMP9/14 activity by recruiting syndecan-1 and CD44. Matrix Biol. 94, 1-17.

Ohuchi E., Imai K., Fujii Y., Sato H., Seiki M. and Okada Y. (1997). Membrane type 1 matrix metalloproteinase digests interstitial collagens and other extracellular matrix macromolecules. J. Biol. Chem. 272, 2446-2451.

Okamoto T., Akaike T., Sawa T., Miyamoto Y., Van Der Vliet A. and Maeda H. (2001). Activation of matrix metalloproteinases by peroxynitrite-induced protein S-Glutathiolation via disulfide S-oxide formation. J. Biol. Chem. 276, 29596-29602.

Piyathilake C.J., Bell W.C., Oelschlager D.K., Heimburger D.C. and Grizzle W.E. (2002). The pattern of expression of Mn and Cu-Zn superoxide dismutase varies among squamous cell cancers of the lung, larynx, and oral cavity. Head Neck 24, 859-867.

Reuter S., Gupta S.C., Chaturvedi M.M. and Aggarwal B.B. (2010). Oxidative stress, inflammation, and cancer: How are they linked? Free Radic. Biol. Med. 49, 1603-1616.

Rosenthal E.L. and Matrisian L.M. (2006). Matrix metalloproteases in head and neck cancer. Head Neck 28, 639-648.

Santos-García A., Abad-Hernández M.M., Fonseca-Sánchez E., Julián-González R., Galindo-Villardón P., Cruz-Hernández J.J. and Bullón-Sopelana A. (2006). E-cadherin, laminin and collagen IV expression in the evolution from dysplasia to oral squamous cell carcinoma. Med. Oral Patol. Oral Cir. Bucal 11, E100-105.

Sato H., Takino T., Okada Y., Cao J., Shinagawa A., Yamamoto E. and Seiki M. (1994). A matrix metalloproteinase expressed on the surface of invasive tumour cells. Nature 370, 61-65.

Sternlicht M.D. and Werb Z. (2001). How matrix metalloproteinases regulate cell behavior. Annu. Rev. Cell Dev. Biol. 17, 463-516.

Sung H., Ferlay J., Siegel R.L., Laversanne M., Soerjomataram I., Jemal A. and Bray F. (2021). Global cancer statistics 2020: GLOBOCAN estimates of incidence and mortality worldwide for 36 cancers in 185 countries. CA Cancer J. Clin. 71, 209-249.

Vivinus-Nebot M., Rousselle P., Breittmayer J.-P., Cenciarini C., Berrih-Aknin S., Spong S., Nokelainen P., Cottrez F., Marinkovich M.P. and Bernard A. (2004). Mature human thymocytes migrate on laminin-5 with activation of metalloproteinase-14 and cleavage of CD44. J. Immunol. 172, 1397-1406.

Wieczorek E., Jablonska E., Wasowicz W. and Reszka E. (2015). Matrix metalloproteinases and genetic mouse models in cancer research: A mini-review. Tumour Biol. 36, 163-175.

Yu F., Kamada H., Niizuma K., Endo H. and Chan P.H. (2008). Induction of MMP-9 expression and endothelial injury by oxidative stress after spinal cord injury. J. Neurotrauma 25, 184-195.

Accepted December 3, 2024